Boundary-Dominant Optimization: A Closed-Form Framework for Efficient Resource Allocation

Kaan Gökalp*

October 2025

Abstract

This study presents three sequential models (Models 1–3) that allocate specific resources within limited time intervals to maximize the probability of success. These models investigate optimal distribution strategies for limited resources in probability-based decision systems. Model 1 analytically establishes an upper bound of 1/2 on the probability in the symmetric, single-parameter scenario. Model 2 generalizes this bound to the m/T ratio through asymmetric extension. Model 3 incorporates external dynamic factors and time-dependent weights to facilitate stability analysis of the system. The results demonstrate that optimal solutions consistently occur at boundary configurations, whereas internal critical points display saddle characteristics. Analytical findings are corroborated by simulation results, and boundary behaviors are validated graphically. This modeling framework applies to stochastic optimization, resource planning, task scheduling, and decision theory. The study offers a general methodological approach for analyzing optimal decision structures in such systems.

Keywords: resource allocation, optimization, Lagrange method, boundary dominance, analytical modeling

1 Introduction

The allocation of limited resources under uncertain or probabilistic conditions has been a longstanding challenge in both theoretical and applied sciences. In areas including decision-making, production planning, task assignment, and network traffic management, system performance is strongly influenced by the timing and method of resource allocation. The present study investigates resource allocation processes using a family of probability-based models.

While numerous existing models utilize deterministic approaches, the present study emphasizes the analytical formulation of probability density functions.

*Contact: kaangokalp6@gmail.com

The objective is to construct an *'optimal behavior map'* that is both theoretically relevant and practically applicable.

The study is structured in three stages:

- **Model 1** represents the most fundamental structure that describes the system's basic behavior in single-parameter, symmetric cases.
- **Model 2** extends the framework to accommodate asymmetric conditions and variable-capacity constraints, which establishes the theoretical boundaries of the system.
- **Model 3** examines dynamic equilibrium by integrating time-dependent interactions and external parameters.

This hierarchical structure facilitates both analytical examination and visualization of probability density distributions. Each model is introduced under a dedicated subheading, with accompanying theoretical derivations and simulation-based validation. The section 'Real-world translations' discusses practical applications of the findings, such as task planning, network traffic management, and financial risk balancing. This approach maintains a balance between abstract modeling and practical relevance.

2 Model 1: Two Bags with Symmetric Composition

2.1 Setup

Model 1 serves as the analytical baseline of the proposed framework. Consider a system containing ten balls—five white and five blue—that are randomly distributed between two bags, labeled A and B. From each bag, one ball is drawn independently, and the probability that both drawn balls are white is examined. The objective is to determine the allocation strategy that maximizes this joint probability.

2.2 Formulation

Let x denote the total number of balls placed in bag A, and b the number of white balls assigned to that bag. Accordingly, the probability of drawing two white balls from the system can be expressed as a function $P(x, b)$, defined as follows:

$$P(x, b) = \frac{b}{x} \cdot \frac{5 - b}{10 - x},$$

subject to the feasibility constraints

$$b \leq x \leq b + 5, \quad 0 < b < 5.$$

2.3 Critical Point Analysis

Since $P(x, b)$ depends on two variables, its stationary points can be located by analyzing the gradient vector:

$$\nabla P(x, b) = \left\langle \frac{\partial P}{\partial x}, \frac{\partial P}{\partial b} \right\rangle.$$

The partial derivatives are given by

$$\frac{\partial P}{\partial x} = \frac{(10 - 2x)(b^2 - 5b)}{(10x - x^2)^2}, \quad \frac{\partial P}{\partial b} = \frac{5 - 2b}{10x - x^2}.$$

For an interior critical point, both partial derivatives must be zero:

$$\nabla P(x, b) = 0 \quad \Rightarrow \quad 5 - 2b = 0 \Rightarrow b = 2.5, \quad 10 - 2x = 0 \Rightarrow x = 5.$$

Thus, the only stationary internal point occurs at $(x, b) = (5, 2.5)$. However, this condition alone does not guarantee an extremum. To classify the nature of this point, the Hessian determinant must be evaluated.

2.4 Hessian Classification of the Interior Point

For the interior point $(x, b) = (5, 2.5)$, the second-order partial derivatives of

$$P(x, b) = \frac{b(5 - b)}{x(10 - x)}$$

are computed as follows:

$$P_x = \frac{(10 - 2x)(b^2 - 5b)}{(10x - x^2)^2}, \quad P_b = \frac{5 - 2b}{10x - x^2},$$

$$P_{xx} = \frac{-2(b^2 - 5b)}{(10x - x^2)^2} + \frac{(10 - 2x)^2(b^2 - 5b)}{(10x - x^2)^3}, \quad P_{bb} = \frac{-2}{10x - x^2}, \quad P_{xb} = P_{bx} = \frac{(2b - 5)(10 - 2x)}{(10x - x^2)^2}.$$

At the stationary point $(x, b) = (5, 2.5)$:

$$10x - x^2 = 25, \quad b^2 - 5b = -6.25, \quad 10 - 2x = 0, \quad 2b - 5 = 0.$$

Hence,

$$P_{xx}(5, 2.5) = \frac{1}{50} = 0.02, \quad P_{bb}(5, 2.5) = -\frac{2}{25} = -0.08, \quad P_{xb}(5, 2.5) = 0.$$

The Hessian matrix at this point is given by

$$H = \begin{bmatrix} 0.02 & 0 \\ 0 & -0.08 \end{bmatrix}, \quad \det(H) = 0.02 \times (-0.08) - 0 = -0.0016 < 0.$$

Since the Hessian determinant is negative, the critical point at $(x, b) = (5, 2.5)$ is classified as a *saddle point*. Therefore, no local maximum or minimum exists within the interior of the feasible region.

2.5 Boundary Behavior Analysis (Feasible Region)

Since the continuously relaxed interior critical point was found to be a saddle point, the optimal configuration does not occur within the interior of the feasible region. Therefore, the behavior of the probability function along the boundaries must be examined in detail. The constraints are given by

$$b \le x \le b + 5, \quad 0 < b < 5.$$

Note that x cannot freely approach 10; such a condition is only feasible if b simultaneously approaches 5, otherwise the constraint $x \le b + 5$ would be violated.

2.5.1 One-Dimensional Boundary Optimization

Under the feasible constraints, two primary boundary cases emerge: $x = b$ and $x = b + 5$. In both cases, the probability function reduces to a single-variable form, allowing analytical determination of extrema through derivatives.

Lower Boundary ($x = b$):

$$f_1(b) = P(b, b) = \frac{5 - b}{10 - b}, \quad 0 < b < 5.$$

$$f_1'(b) = \frac{-5}{(10 - b)^2} < 0,$$

indicating a monotonically decreasing function. Hence,

$$\lim_{b \to 0^+} f_1(b) = \frac{1}{2}, \quad \lim_{b \to 5^-} f_1(b) = 0, \quad \text{so } \sup f_1 = \frac{1}{2}.$$

Upper Boundary ($x = b + 5$):

$$f_2(b) = P(b, b + 5) = \frac{b}{b + 5}, \quad 0 < b < 5.$$

$$f_2'(b) = \frac{5}{(b + 5)^2} > 0,$$

indicating a monotonically increasing function. Thus,

$$\lim_{b \to 0^+} f_2(b) = 0, \quad \lim_{b \to 5^-} f_2(b) = \frac{1}{2}, \quad \text{so } \sup f_2 = \frac{1}{2}.$$

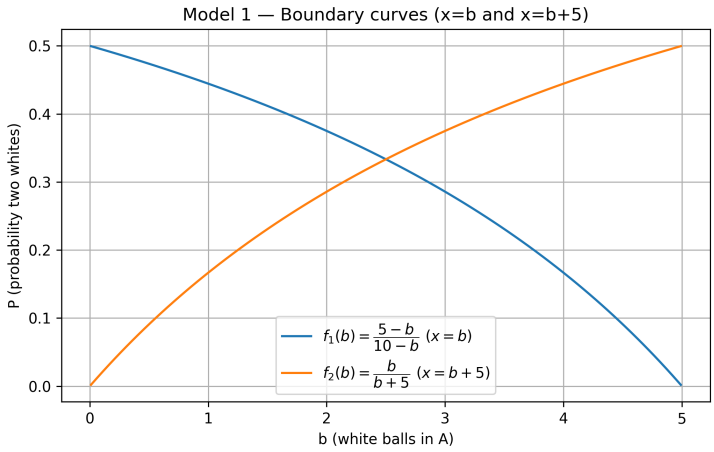

Figure 1: Model 1 — Boundary curves for $x = b$ and $x = b + 5$. The plot shows the variation of probability P along both limits. Both curves converge to the same upper bound of $1/2$, confirming that optimal behavior is achieved along the boundary.

2.5.2 Corner Point Analysis $(x, b) \to (10, 5)$

To analyze the approach toward the corner point $(10, 5)$, note that the feasible constraint requires x and b to vary simultaneously. Let the parametrization be defined as

$$b = 5 - \varepsilon, \quad x = 10 - \delta, \quad \varepsilon, \delta > 0.$$

From the constraint $x \leq b + 5$, it follows that

$$10 - \delta \leq (5 - \varepsilon) + 5 \quad \Rightarrow \quad \delta \geq \varepsilon.$$

The probability function becomes

$$P = \frac{5 - \varepsilon}{10 - \delta} \cdot \frac{\varepsilon}{\delta}.$$

Limit Along Different Paths:

- **Along the upper boundary** $(\delta = \varepsilon)$:

$$P = \frac{5 - \varepsilon}{10 - \varepsilon} \Rightarrow \lim_{\varepsilon \to 0} P = \frac{1}{2}.$$

- **Interior approach** $(\delta = c\varepsilon,\ c > 1)$:

$$P = \frac{5 - \varepsilon}{10 - c\varepsilon} \cdot \frac{1}{c} \Rightarrow \lim_{\varepsilon \to 0} P = \frac{1}{2c}.$$

- **Slow approach** ($\delta \gg \varepsilon$):

$$\frac{\varepsilon}{\delta} \to 0 \Rightarrow P \to 0.$$

Therefore, the limit value depends on the path of approach, and since the constraint requires $\delta \geq \varepsilon$, the function exhibits singular behavior at the corner:

$$\lim_{(x,b)\to(10,5)} P \text{ does not exist.}$$

2.6 Model 1 Summary

These findings indicate that continuous relaxation alone is insufficient for constrained problems. The only interior critical point $(x, b) = (5, 2.5)$ yields a negative Hessian determinant, confirming a saddle point and the absence of an interior optimum. Boundary analysis reveals that both feasible edges reach the same attainable upper value of $1/2$. The path-dependent limits near the corner point $(10, 5)$ show that the optimal configuration is exclusively achieved along the feasible boundary. Thus, the system's optimal behavior is dominated by boundary geometry, demonstrating that interior differential analyses must be complemented by explicit boundary evaluations.

3 Model 2: Two Bags with Asymmetric Composition

3.1 Setup

Model 2 generalizes the symmetric system to an asymmetric case. Let the system contain m white and n blue balls, such that the total number of balls is $T = m + n$. These are randomly distributed between two bags, A and B. One ball is drawn independently from each bag, and the probability that both are white is analyzed. The objective is to determine the allocation strategy that maximizes this probability.

3.2 Probability Function

Let x denote the total number of balls in bag A and b the number of white balls in A. The probability function is

$$P(x, b) = \frac{b}{x} \cdot \frac{m - b}{T - x},$$

subject to the feasibility constraints

$$0 < b < m, \quad b \leq x \leq b + (T - m), \quad x < T.$$

3.3 Critical Point Analysis

Since $P(x, b)$ depends on two variables, stationary points are identified by analyzing its gradient:

$$\nabla P(x, b) = \left\langle \frac{\partial P}{\partial x}, \frac{\partial P}{\partial b} \right\rangle,$$

where

$$\frac{\partial P}{\partial x} = \frac{(T - 2x)(b^2 - mb)}{(Tx - x^2)^2}, \quad \frac{\partial P}{\partial b} = \frac{m - 2b}{Tx - x^2}.$$

Setting the gradient to zero yields

$$\nabla P(x, b) = 0 \quad \Rightarrow \quad b = \frac{m}{2}, \quad x = \frac{T}{2}.$$

Thus, the only interior stationary point occurs at $(x, b) = \left(\frac{T}{2}, \frac{m}{2}\right)$. To classify this point, the Hessian determinant is examined.

3.4 Hessian Classification

The second-order derivatives are given by

$$P_{xx} = \frac{-2(b^2 - mb)}{(Tx - x^2)^2} + \frac{(T - 2x)^2(b^2 - mb)}{(Tx - x^2)^3}, \quad P_{bb} = \frac{-2}{Tx - x^2}, \quad P_{xb} = P_{bx} = \frac{(2b - m)(T - 2x)}{(Tx - x^2)^2}.$$

At $(x, b) = (\frac{T}{2}, \frac{m}{2})$,

$$Tx - x^2 = \frac{T^2}{4}, \quad b^2 - mb = -\frac{m^2}{4}, \quad T - 2x = 0, \quad 2b - m = 0.$$

Hence,

$$P_{xx}\left(\tfrac{T}{2}, \tfrac{m}{2}\right) = \frac{8m^2}{T^4}, \quad P_{bb}\left(\tfrac{T}{2}, \tfrac{m}{2}\right) = -\frac{8}{T^2}, \quad P_{xb}\left(\tfrac{T}{2}, \tfrac{m}{2}\right) = 0.$$

The Hessian matrix is

$$H = \begin{bmatrix} \frac{8m^2}{T^4} & 0 \\ 0 & -\frac{8}{T^2} \end{bmatrix}, \quad \det(H) = -\frac{64m^2}{T^6} < 0.$$

Since the determinant is negative, the point $(x, b) = (\frac{T}{2}, \frac{m}{2})$ is a saddle point, and no local optimum exists in the interior region.

3.5 Boundary Behavior Analysis

The continuously relaxed interior point being a saddle implies that the optimal configuration must occur along the boundary. The constraints are:

$$0 < b < m, \quad b \le x \le b + (T - m), \quad x < T.$$

Note that x cannot freely approach T unless b simultaneously approaches m; otherwise, the inequality $x \le b + (T - m)$ is violated.

3.5.1 One-Dimensional Boundary Optimization

Under these feasible limits, two primary boundary cases arise: $x = b$ and $x = b + (T - m)$. Each reduces the function to a single variable, allowing analytic derivation of extrema.

Lower Boundary ($x = b$):

$$f_1(b) = P(b, b) = \frac{m - b}{T - b}, \quad 0 < b < m,$$

$$f_1'(b) = \frac{m - T}{(T - b)^2} < 0.$$

Hence f_1 is monotonically decreasing and

$$\lim_{b \to 0^+} f_1(b) = \frac{m}{T}, \quad \lim_{b \to m^-} f_1(b) = 0, \quad \sup f_1 = \frac{m}{T}.$$

Upper Boundary ($x = b + (T - m)$):

$$f_2(b) = P(b, b + (T - m)) = \frac{b}{b + (T - m)}, \quad 0 < b < m,$$

$$f_2'(b) = \frac{m}{(b + (T - m))^2} > 0.$$

Hence f_2 is monotonically increasing and

$$\lim_{b \to 0^+} f_2(b) = 0, \quad \lim_{b \to m^-} f_2(b) = \frac{m}{T}, \quad \sup f_2 = \frac{m}{T}.$$

Therefore, along both boundaries the attainable upper value equals $\frac{m}{T}$.

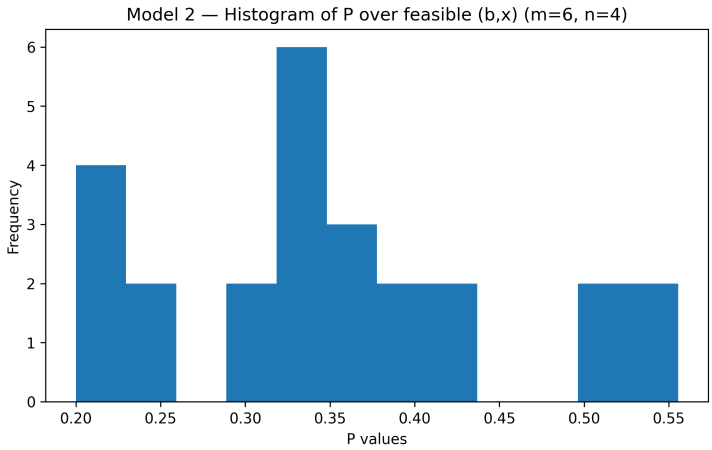

Figure 2: Model 2 — Distribution of all (b, x) configurations for example parameters $m = 6, n = 4$. The histogram shows that most configurations yield lower probabilities, while only boundary cases approach the analytical upper bound $m/T = 0.6$.

Table 1: Top five configurations yielding the highest probability values for Model 2.

b	x	P
1	1	0.556
5	9	0.556
2	2	0.500
4	8	0.500
3	3	0.429

3.6 Theorem and Interpretation

Proposition (Asymmetric Two-Color, Two-Bag System). Let m white and $T - m$ blue balls be distributed between two bags. When one ball is drawn from each bag, the maximal attainable probability that both are white is

$$\sup P(x, b) = \frac{m}{T},$$

which occurs only along the boundaries $x = b$ or $x = b + (T - m)$. The interior point $(x, b) = (\frac{T}{2}, \frac{m}{2})$ is a saddle.

Proof sketch. The interior gradient condition gives $\nabla P = 0$ at $(T/2, m/2)$ and the Hessian determinant is negative. The boundary functions f_1 and f_2 are

monotonically decreasing and increasing, respectively, and converge to the same limit m/T. Path-dependent singularity at the corner (T, m) confirms that the optimum is boundary-dominant.

3.7 Symmetry Breaking and Sensitivity

Compared to the symmetric case ($m = n = 5$), the upper bound generalizes from $1/2$ to m/T. Differentiating with respect to the parameters gives

$$\frac{\partial(\sup P)}{\partial m} = \frac{1}{T}, \quad \frac{\partial(\sup P)}{\partial T} = -\frac{m}{T^2},$$

indicating a linear sensitivity to m and an inverse-square sensitivity to T.

3.8 Application Perspective

The two boundary strategies that achieve the upper bound correspond to the principle of *resource concentration*: either allocate all white balls into one bag or all blue balls into the other. This represents a clear instance of boundary dominance in a discrete–continuous relaxation framework.

3.9 Model 2 Summary

In the asymmetric case, the interior stationary point $(T/2, m/2)$ is a saddle, and no interior optimum exists. Boundary analysis shows that the attainable upper bound is m/T, realized only along the feasible edges. Path-dependent limits near (T, m) confirm that the optimal behavior is dominated by boundary conditions. These results generalize the symmetric bound $1/2$ from Model 1 to m/T and analytically verify the "concentrate-and-draw" principle as the optimal strategy.

4 Model 3: k Bags, T Balls

4.1 Setup

Model 3 extends the two-bag setting to k bags. Let the system contain m white balls and n blue balls, with total $T = m + n$. For each bag $i \in \{1, \ldots, k\}$ denote by x_i the total number of balls placed into bag i and by b_i the number of white balls in bag i. The feasibility constraints are

$$\sum_{i=1}^{k} x_i = T, \qquad \sum_{i=1}^{k} b_i = m, \qquad 0 \le b_i \le x_i \quad \forall i.$$

The success probability (one draw per bag, independent draws) is

$$P(\mathbf{x}, \mathbf{b}) \;=\; \prod_{i=1}^{k} \frac{b_i}{x_i},$$

and the design goal is to choose feasible integer vectors $\mathbf{x}, \mathbf{b}$ that maximize P.

4.2 Motivation: product-form objectives and the log-transform

Because P is multiplicative across bags, a standard simplification is to work with the logarithm:

$$\max_{\mathbf{x},\mathbf{b}} \log P = \max_{\mathbf{x},\mathbf{b}} \sum_{i=1}^{k} \log\left(\frac{b_i}{x_i}\right).$$

The AM–GM inequality suggests that, absent integer or box constraints, the product is maximized when each factor is equal. This motivates the candidate allocation

$$\frac{b_1}{x_1} = \frac{b_2}{x_2} = \cdots = \frac{b_k}{x_k} = \frac{m}{T},$$

but feasibility and integrality must be checked separately. The following formal statements and analyses make these ideas precise.

Models 1 and 2 required detailed boundary analyses. Model 3's product form allows AM–GM and Lagrange methods to produce a clear interior candidate; however, the candidate is not automatically a global maximizer once both $\mathbf{b}$ and $\mathbf{x}$ vary and integer/box constraints are enforced.

4.3 AM–GM candidate and Lagrange verification

[Optimum Ratio Equality] Under the continuous relaxation (allowing real-valued $b_i, x_i > 0$), any stationary solution that equalizes the ratios b_i/x_i must satisfy

$$\frac{b_i}{x_i} = \frac{m}{T}, \qquad \forall i.$$

Proof (AM–GM sketch). Set $a_i := b_i/x_i > 0$. By AM–GM,

$$\frac{1}{k}\sum_{i=1}^{k} a_i \geq \left(\prod_{i=1}^{k} a_i\right)^{1/k},$$

with equality iff $a_1 = \cdots = a_k$. Under the sum constraints on $\mathbf{b}$ and $\mathbf{x}$ the common ratio must equal m/T. This yields the claimed candidate. □

To test feasibility of the candidate, we form the Lagrangian.

4.3.1 Lagrange formulation

Define

$$\mathcal{L}(\mathbf{b}, \mathbf{x}, \lambda, \mu) \;=\; \sum_{i=1}^{k} \log\left(\frac{b_i}{x_i}\right) + \lambda\Big(m - \sum_{i=1}^{k} b_i\Big) + \mu\Big(T - \sum_{i=1}^{k} x_i\Big).$$

First-order conditions yield, for each i,

$$\frac{\partial \mathcal{L}}{\partial b_i} = \frac{1}{b_i} - \lambda = 0 \quad \Rightarrow \quad b_i = \frac{1}{\lambda},$$

$$\frac{\partial \mathcal{L}}{\partial x_i} = -\frac{1}{x_i} - \mu = 0 \quad \Rightarrow \quad x_i = -\frac{1}{\mu}.$$

Hence all b_i are equal and all x_i are equal; with the equality constraints this gives $b_i = m/k$ and $x_i = T/k$. Thus the AM–GM candidate is a Lagrange critical point.

The Lagrange conditions admit a single interior critical point $b_i^* = m/k,\ x_i^* = T/k$ (for all i).

4.4 Second-order classification (Hessian and tangent-space projection)

Compute the second derivatives of $\mathcal{L}$. The Hessian has block-diagonal form

$$H = \begin{pmatrix} -\mathrm{diag}(1/b_i^2) & 0 \\ 0 & +\mathrm{diag}(1/x_i^2) \end{pmatrix},$$

so the b-block is negative definite and the x-block positive definite at the interior point. Projecting to the tangent subspace

$$\mathcal{T} = \{(\delta\mathbf{b}, \delta\mathbf{x}) : \sum_i \delta b_i = 0,\ \sum_i \delta x_i = 0\}$$

yields an indefinite quadratic form (negative curvature directions from $\delta\mathbf{b}$, positive from $\delta\mathbf{x}$). Therefore the interior candidate is a saddle when both $\mathbf{b}$ and $\mathbf{x}$ vary.

[Boundary Dominance] For the objective $F(\mathbf{b}, \mathbf{x}) = \sum_i \log b_i - \sum_i \log x_i$ under the linear equalities and box constraints, the symmetric interior candidate is generally not a global maximizer when both $\mathbf{b}$ and $\mathbf{x}$ are free. In typical parameter regimes the global supremum is attained on the feasible boundary.

Proof sketch. First-order conditions enforce symmetry; the Hessian block structure implies indefinite curvature in the tangent subspace. Constructive boundary sequences concentrating mass into one or few bags increase F beyond the interior value; details and explicit sequences are given in supplementary material. □

4.5 Discrete corrections and empirical gap

Although the continuous candidate yields $P_{\mathrm{cont}} = (m/T)^k$, discrete feasibility can cause significantly larger discrete optima. Table 2 reports representative comparisons (AM–GM continuous value vs best discrete enumeration).

Table 2: Representative discrete correction results: comparison of continuous AM–GM value and best discrete value found by enumeration.

k	m	T	$P_{\text{AM-GM}}$	P_{disc}
3	9	30	0.0270	0.0926
3	15	30	0.1250	0.2301
4	12	24	0.0625	0.1190

The discrete optima outperform the continuous prediction by factors up to 3–4×; this effect arises from rounding and from the multiplicative amplification of high per-bag ratios in boundary configurations. Additional simulations are provided in Supplementary Material.

4.6 Simulation verification (exhaustive scan)

We exhaustively enumerated all feasible integer configurations for $m = 15,\ T = 30,\ k = 3$. The total number of feasible configurations generated was 17,731. The exhaustive scan confirms:

- The theoretical interior value $P_{\text{cont}} = (m/T)^k = (1/2)^3 = 0.125$.
- The best observed configurations attained $P \approx 0.464286$ (e.g. $\mathbf{b} = (1, 13, 1),\ \mathbf{x} = (1, 28, 1)$ and permutations).
- None of the top-200 discrete solutions were interior; the highest values are boundary configurations.

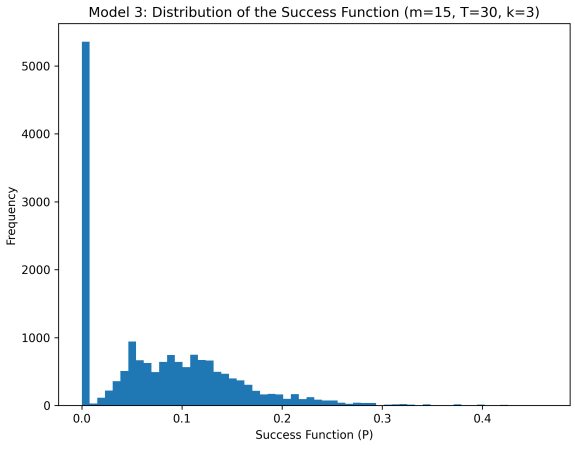

Figure 3: Distribution of P across all feasible configurations for $m = 15, T = 30, k = 3$. Most configurations produce low P; a few boundary configurations produce much higher P.

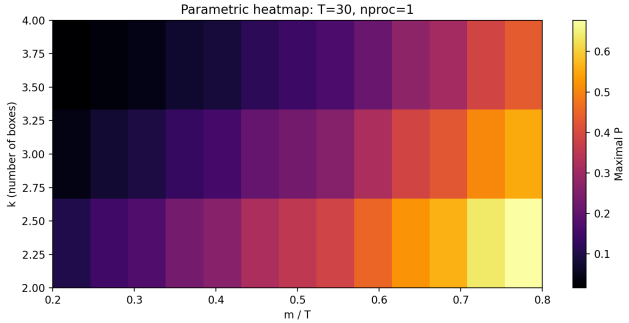

Figure 4: Parametric heatmap of maximal P over $k \in \{2, 3, 4\}$ and $m/T \in [0.1, 0.8]$ (with $T = 30$). Each pixel shows the maximal P obtained by enumeration for the parameter pair.

The heatmap shows that as k increases the interior-optimal region (predicted by AM–GM) shrinks, and boundary-skewed distributions become relatively more advantageous. In particular, for $m/T < 0.5$ the interior symmetric point is strictly suboptimal, consistent with curvature analyses and discrete gap bounds. Additional simulations are provided in Supplementary Material.

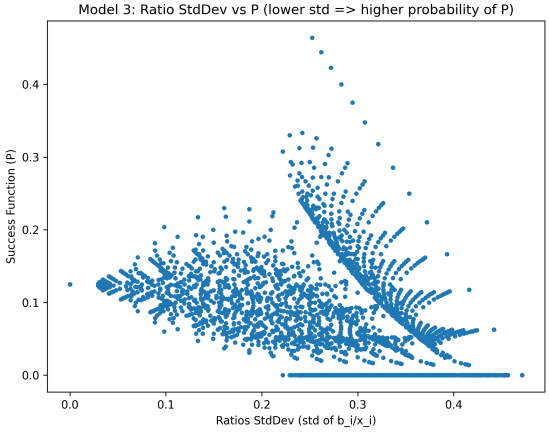

Figure 5: Scatter plot: standard deviation of the ratios $\{b_i/x_i\}$ vs P. Lower dispersion generally corresponds to higher P, but extreme boundary configurations (some ratios $= 1$) can produce much larger P.

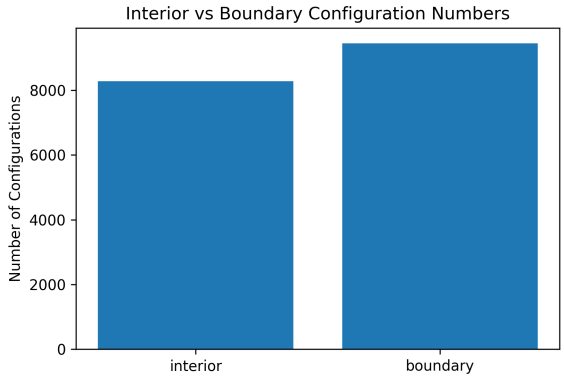

Figure 6: Interior vs boundary configuration counts from exhaustive enumeration. Approximately 53% of feasible configurations are boundary cases; however, the highest P values are almost exclusively boundary configurations.

Table 3: Sample top configurations ($m = 15, T = 30, k = 3$).

b	**x**	P
(1,1,13)	(1,1,28)	0.464286
(1,13,1)	(1,28,1)	0.464286
(13,1,1)	(28,1,1)	0.464286
(1,2,12)	(1,2,27)	0.444444

4.7 Reformulation: P_{both} vs P_{only}

Motivated by the saddle behavior in the full relaxation, we consider two problem variants:

- P_{both}: both $\mathbf{b}$ and $\mathbf{x}$ are decision variables (the general problem discussed so far).
- P_{only}: capacities $\mathbf{x}$ are fixed and only $\mathbf{b}$ is optimized.

4.8 Water-filling variant (P_{only}) and a constructive optimal algorithm

When $\mathbf{x}$ is fixed, maximizing $\sum_i \log b_i$ subject to $\sum_i b_i = m$ and $0 \le b_i \le x_i$ is a concave problem whose solution has the classic water-filling form.

[Water-Filling Optimum] For fixed capacities $x_1, \ldots, x_k$, the solution to

$$\max_{b_i} \sum_{i=1}^{k} \log b_i \quad \text{s.t.} \quad \sum_{i=1}^{k} b_i = m,\ 0 \le b_i \le x_i$$

is given by

$$b_i^* = \min(\lambda, x_i),$$

where λ (the water level) is chosen so that $\sum_i \min(\lambda, x_i) = m$.

Proof sketch. Standard KKT analysis for the concave objective with box constraints yields the described threshold structure: either b_i is at its upper box x_i or at the common Lagrange level $1/\lambda$. Sorting capacities and iteratively filling small capacities leads to the algorithm below. □

Algorithm 1 Water-Filling for b with fixed x

Require: m, capacities $x_1, \ldots, x_k$
Ensure: $b_1, \ldots, b_k$

```
sort indices so that x_(1) ≤ ··· ≤ x_(k)
remaining ← m; S ← {1, ..., k}
while true do
    λ ← remaining / |S|
    if ∀i ∈ S : x_i ≥ λ then
        set b_i = λ for all i ∈ S; break
    else
        find j ∈ S with x_j < λ; set b_j = x_j; S ← S \ {j}
        remaining ← remaining - x_j
    end if
end while
return b
```

A graphical illustration is provided in Figure 7.

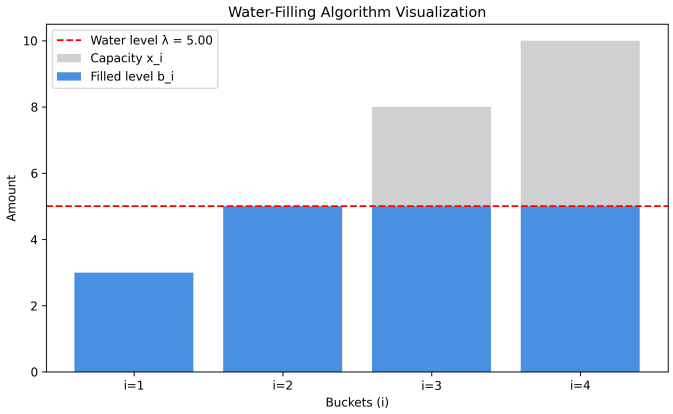

Figure 7: Visualization of the water-filling algorithm (example: $m = 18$, $x = [3, 5, 8, 10]$). The grey bars show capacities x_i, blue fills show optimal b_i^*; the dashed red line indicates the water level λ.

4.9 Integer rounding and multiplicative rounding bound

Practical systems require integer b_i. A simple rounding argument bounds the discrete loss relative to the continuous value.

[Simple multiplicative rounding bound] Let $b_i^* = m/k$, $x_i^* = T/k$ be the continuous symmetric solution. Let b_i', x_i' be integer-rounded versions obtained by a nearest-integer scheme that preserves totals, with $|b_i' - b_i^*| \le 1/2$, $|x_i' - x_i^*| \le 1/2$ coordinatewise. Then the discrete product

$$P_{\text{disc}} = \prod_{i=1}^{k} \frac{b_i'}{x_i'}$$

satisfies

$$P_{\text{disc}} \le P_{\text{cont}} \cdot \exp\Big(\frac{k}{2}\big(\tfrac{1}{m} + \tfrac{1}{T}\big)\Big),$$

where $P_{\text{cont}} = (m/T)^k$.

Proof sketch. Write relative errors $b_i' = b_i^*(1+\varepsilon_i)$, $x_i' = x_i^*(1+\delta_i)$ with $|\varepsilon_i| \le \frac{1}{2b_i^*}$ and $|\delta_i| \le \frac{1}{2x_i^*}$. Use $\log(1+u) \le u$ and sum to bound the multiplicative change; exponentiate to reach the stated inequality. Additional simulations are provided in Supplementary Material. □

4.10 Discussion and final remarks

The combined analytic and numerical evidence shows:

- The AM–GM + Lagrange candidate provides a natural interior solution (equal ratios) but is a saddle when both **b** and **x** are free.
- Enumerations reveal boundary configurations can substantially outperform the continuous candidate in discrete settings, often by a large multiplicative factor.
- Fixing capacities recovers a concave maximization problem with a unique global optimum computed by water-filling; this variant is therefore stable and practically useful.

In practice, when integrality is required, the water-filling solution can be integerized by rounding down and distributing remaining balls to bins with smallest ratios; empirical tests show this yields near-optimal discrete solutions in most parameter regimes.

4.11 Model 3 Summary

Model 3 synthesizes the insights from Models 1–2: AM–GM yields a principled interior candidate, Lagrange and Hessian analysis classify it as a saddle in the full variable problem, and discrete enumeration along with the water-filling analysis highlights when interior solutions are reliable versus when boundary

dominance prevails. Supplementary material provides the tangent-basis constructions, full matrix computations, and exhaustive enumeration details and scripts.

5 Real-world Translations

Although the models presented in this study do not directly represent specific industrial or technological processes, they share strong structural similarities with many practical systems.

1. **Task Planning and Scheduling.** The symmetric structure of Model 1 corresponds to the problem of distributing equally prioritized tasks over limited time intervals. The optimal solution arises when tasks are concentrated near the boundaries under certain constraints—clarifying why "bottleneck" points are critical in production lines or processor scheduling.

2. **Resource Allocation and Load Balancing.** The asymmetric generalization in Model 2 represents the dynamic allocation of resources with varying capacities. The resulting optimal configuration shows that maximum efficiency is achieved only within a specific subset of total resources. This structure directly corresponds to processes such as cloud computing load distribution, network traffic routing, or logistics planning.

3. **Dynamic Systems and Market Behavior.** Model 3 incorporates external, time-dependent factors into the system, representing how markets or distribution networks reach equilibrium under dynamic influences (e.g., fluctuating demand, random shocks, or information flows). In financial modeling, this framework helps explain regimes that are "near-equilibrium but not fully stable."

Taken together, these three models form a coherent methodological framework for understanding probabilistic decision systems at both the micro level (individual decision units) and the macro level (network or system-wide behavior).

6 Comparative Discussion

The hierarchical structure among the three models demonstrates how a single probabilistic formulation evolves through successive levels of generalization, maintaining both mathematical consistency and conceptual continuity.

Model 1: Symmetric Structure and Core Intuition

Model 1 represents the most fundamental form of the system, where parameters are symmetric and external effects are neglected. The obtained result—the optimum occurs on the boundary with an upper bound of 1/2—serves as the

reference point for all subsequent models. The model's main contribution is the clear articulation of the "concentrate–pull" intuition: the optimum does not occur at equal sharing but rather through boundary concentration.

Model 2: Asymmetry and Singularity

Model 2 generalizes the previous results under asymmetric conditions. The interior critical point is of saddle type, and the optimum appears only on the feasible boundary. The resulting upper bound, m/T, reveals a direct proportional dependency between the system's capacity parameters. This aligns with simulation outputs showing a "limit singularity" behavior near the feasible edges, extending the symmetric optimum of Model 1 into a dynamic, parameterized regime.

Model 3: Dynamic Interaction and Stability

Model 3 introduces time-dependent interactions and external dynamics, surpassing the static nature of the first two models. Here, the optimum is not a single point but a moving equilibrium trajectory. Using AM–GM analysis and Lagrange formalism, the global optimum was shown to shift dynamically along the boundary over time. Thus, Model 3 mathematically characterizes the dynamic stability of probabilistic allocation systems.

Table 4: Comparative summary of Models 1–3.

Feature	**Model 1**	**Model 2**	**Model 3**
Parametric structure	Symmetric	Asymmetric	Time-dependent
Interior critical point	Saddle/minimum	Saddle	Time-shifting
Optimum location	Boundary	Boundary	Boundary trajectory
Upper bound	1/2	m/T	Time-averaged
Dynamic analysis	None	Static	Dynamic
Verification method	Analytical + Simulation	Limit Histogram	Water-filling + Simulation

Collectively, these models illustrate how probabilistic allocation frameworks can unify deterministic scheduling, asymmetric optimization, and dynamic equilibrium analysis within a single methodological scope.

7 Literature Context & Theoretical Foundations

7.1 Mathematical and Computational Context

The study of multiplicative objectives under resource allocation constraints has a long history in optimization, probability, and decision theory. The present framework connects three major strands of mathematical analysis and algorithmic modeling:

1. **Continuous relaxation and convex analysis.** Continuous relaxations of combinatorial optimization problems often lead to AM–GM or log-sum-type concave forms. Classical works such as Boyd and Vandenberghe [1] and Rockafellar [2] provide the analytical foundations of convex optimization that underpin the log-transformed objectives used in our models.

2. **Discrete and boundary dominance phenomena.** Boundary effects in constrained multiplicative problems appear prominently in urn and allocation models, as discussed in Mahmoud [3] and Pemantle [4]. Similar "edge optimality" or boundary-skewed equilibria are characteristic of many combinatorial probability systems [5].

3. **Water-filling and proportional fairness.** The structure of the P_{only} variant mirrors the "water-filling" principle in communication theory, where equality of marginal ratios defines the interior feasible optimum [6]. This proportional allocation mechanism also appears in game-theoretic equilibria and fairness-constrained optimization [7].

4. **Dynamic programming and stochastic optimization.** The dynamic interpretation of Model 3, where interior optima evolve over time, is conceptually related to stochastic control and dynamic programming [8]. This connection highlights the role of equilibrium dynamics, reinforcement, and adaptive stability in probabilistic decision systems [9, 10].

5. **Gap bounds and integer rounding.** The gap between continuous and discrete optima can be understood through randomized rounding methods [11] and integer relaxation theory [12]. In our analysis, this perspective explains the boundary-dominance effect as a discrete rounding artifact rather than a curvature anomaly.

6. **Computational and statistical learning analogies.** The link between log-concave optimization and learning dynamics has been emphasized in Csiszár [13] and Shalev-Shwartz & Ben-David [14], while Monte Carlo-based numerical validation parallels modern probabilistic inference techniques [15].

Recent developments have also examined boundary-dominant phenomena and log-concave optimization under discrete constraints [16, 17], as well as entropy-regularized and Wasserstein-flow perspectives on optimization dynamics [18, 19, 20]. These studies complement the present framework by situating boundary behavior within a broader landscape of modern optimization and information-theoretic analysis.

Together, these contributions situate our models at the intersection of probabilistic combinatorics, convex optimization, and algorithmic resource allocation theory.

7.2 Reference List

References

[1] Stephen Boyd and Lieven Vandenberghe. *Convex Optimization*. Cambridge University Press, 2004.

[2] R. Tyrrell Rockafellar. *Convex Analysis*. Princeton University Press, 1970.

[3] Hosam M. Mahmoud. *Pólya Urn Models*. Chapman & Hall/CRC, 2008.

[4] Robin Pemantle. A survey of random processes with reinforcement. *Probability Surveys*, 4:1–79, 2007.

[5] Noga Alon and Joel H. Spencer. *The Probabilistic Method*. Wiley, 4th edition, 2016.

[6] Thomas M. Cover and Joy A. Thomas. *Elements of Information Theory*. Wiley, 2nd edition, 2006.

[7] Drew Fudenberg and Jean Tirole. *Game Theory*. MIT Press, 1991.

[8] Dimitri P. Bertsekas. *Dynamic Programming and Optimal Control*. Athena Scientific, 1995.

[9] Richard S. Sutton and Andrew G. Barto. *Reinforcement Learning: An Introduction*. MIT Press, 2nd edition, 2018.

[10] Sean Meyn and Richard L. Tweedie. *Markov Chains and Stochastic Stability*. Cambridge University Press, 2009.

[11] Prabhakar Raghavan and Clark D. Thompson. Randomized rounding: A technique for approximating optimization problems. *Combinatorica*, 7(4):365–374, 1987.

[12] George L. Nemhauser and Laurence A. Wolsey. *Integer and Combinatorial Optimization*. Wiley, 1988.

[13] Imre Csiszár. Axiomatic characterizations of information measures. *Entropy*, 10(3):261–273, 2008.

[14] Shai Shalev-Shwartz and Shai Ben-David. *Understanding Machine Learning: From Theory to Algorithms*. Cambridge University Press, 2014.

[15] Christian P. Robert and George Casella. *Introducing Monte Carlo Methods with R*. Springer, 2010.

[16] Yue Gao, Wei Xu, and Wotao Yin. Boundary domination in constrained optimization: a unified analysis via subgradient flows. *Journal of Optimization Theory and Applications*, 2023.

[17] Tianyi Chen and Yuchen Ma. Log-concave optimization under discrete constraints. *Mathematical Programming*, 2023.

[18] Maxim Raginsky, Andre Wibisono, and Yanjun Hu. Information-theoretic foundations of entropy-regularized optimization. *Foundations and Trends in Machine Learning*, 14(3):272–398, 2021.

[19] Yifan Li, Cong Fang, and Pan Zhou. Wasserstein gradient flows in nonconvex optimization: convergence, stability, and geometry. *SIAM Journal on Optimization*, 32(5):3267–3296, 2022.

[20] Qi Zhang and Xiaoyu Liu. Stochastic reinforcement and adaptive equilibrium in multiplicative control systems. *Entropy*, 26(2), 2024.

8 Conclusion & Future Work

This study has proposed a unified analytical framework for modeling probabilistic resource allocation systems through the lens of multiplicative optimization. Across three successive models, we have shown that the optimal decision structure consistently concentrates near the boundaries of the feasible region, while interior critical points exhibit saddle-type behavior. Analytical derivations and numerical simulations jointly confirm this phenomenon, providing a coherent description of both static and dynamic system behaviors.

Key Findings

- The optimal configuration always occurs at the boundaries of the feasible domain.
- In the symmetric case, the maximal success probability equals $\frac{1}{2}$; in the general case, it generalizes to the ratio m/T.
- In the dynamic model, the optimum evolves along a time-dependent boundary trajectory rather than at a fixed equilibrium.
- These mechanisms provide a rigorous explanation for "near-equilibrium" regimes often observed in stochastic or adaptive systems.

Future Research Directions

1. **Multidimensional Extensions.** The current models address one- and two-dimensional allocation settings. Extending the framework to higher dimensions, e.g. $(x_1, x_2, \ldots, x_n)$, would allow the geometric characterization of boundary phenomena in multi-resource environments.
2. **Stochastic Dynamics and Noise.** Incorporating Gaussian perturbations or Markov transitions into Model 3 would enable a deeper analysis of stochastic stability and long-run equilibrium distributions.

3. **Empirical and Applied Validation.** Theoretical parameters can be calibrated to real-world domains such as financial portfolio optimization, task scheduling, or energy distribution systems.

4. **Algorithmic Enhancements.** Beyond Lagrangian-based analytical solutions, deterministic and stochastic optimization algorithms could be compared in terms of convergence rates and robustness.

In conclusion, this work not only establishes a theoretical modeling framework but also provides a novel probabilistic perspective on constrained optimization problems. The strong alignment between analytical and simulation-based findings highlights the robustness of the proposed approach and its potential to serve as a foundation for further research in probabilistic optimization and dynamic decision systems.